# Solar influence on climate during the past millennium: Results from transient simulations with the NCAR Climate System Model

Caspar M. Ammann*, Fortunat Joos*†‡, David S. Schimel*, Bette L. Otto-Bliesner*, and Robert A. Tomas*

*Climate and Global Dynamics Division, National Center for Atmospheric Research, 1850 Table Mesa Drive, Boulder, CO 80307-3000; and †Climate and Environmental Physics, Physics Institute, University of Bern, Sidlerstrasse 5, CH-3012 Bern, Switzerland

Communicated by Stephen H. Schneider, Stanford University, Stanford, CA, June 28, 2006 (received for review February 27, 2006)

**The potential role of solar variations in modulating recent climate has been debated for many decades and recent papers suggest that solar forcing may be less than previously believed. Because solar variability before the satellite period must be scaled from proxy data, large uncertainty exists about phase and magnitude of the forcing. We used a coupled climate system model to determine whether proxy-based irradiance series are capable of inducing climatic variations that resemble variations found in climate reconstructions, and if part of the previously estimated large range of past solar irradiance changes could be excluded. Transient simulations, covering the published range of solar irradiance estimates, were integrated from 850 AD to the present. Solar forcing as well as volcanic and anthropogenic forcing are detectable in the model results despite internal variability. The resulting climates are generally consistent with temperature reconstructions. Smaller, rather than larger, long-term trends in solar irradiance appear more plausible and produced modeled climates in better agreement with the range of Northern Hemisphere temperature proxy records both with respect to phase and magnitude. Despite the direct response of the model to solar forcing, even large solar irradiance change combined with realistic volcanic forcing over past centuries could not explain the late 20th century warming without inclusion of greenhouse gas forcing. Although solar and volcanic effects appear to dominate most of the slow climate variations within the past thousand years, the impacts of greenhouse gases have dominated since the second half of the last century.**

Understanding and quantifying natural climate variability on decadal to centennial time scales is a prerequisite to project future climate changes. It is important to evaluate comprehensive models in the preindustrial period when natural variations were (relatively) pronounced and anthropogenic influences were comparatively small. The recently improved records of the variations in climate of the past 1,000 years (1) together with solar and volcanic forcing histories (2, 3) provide a key opportunity for (*i*) evaluating long transient simulations with Atmosphere–Ocean General Circulation Models over the preindustrial era, (*ii*) for exploring the proposed magnitudes of past solar irradiance changes, and (*iii*) to estimate natural contributions to century-scale climate variability.

A range of Northern Hemisphere (NH) and one global surface temperature reconstructions for the past millennium have become available in the past few years. These studies infer the magnitude of past temperature variations from networks of proxy data, such as tree ring width and density, coral growth, ice core, speleothem, and documentary data or from borehole temperature profiles. Each method, in combination with its specific data network, suffers from a variety of uncertainties (see discussion in ref. 1) and, especially at longer time scales, individual temperature series deviate notably from each other. This is particularly the case for the magnitude of the cooling during the repeated intervals (interrupted by warmer decades) encompassing what is generally referred to as the Little Ice Age, ≈1300–1850 AD. However, most maintain a similar temporal structure, and taken together they suggest that natural century scale NH-temperature variations over the past millennium remained within 0.3°C (low estimate in refs. 4 and 5) to ≈1°C (high estimate, e.g., refs. 6–8). Southern hemisphere temperature estimates exist (1, 9), but they are hampered by restricted data coverage.

The dominating hypotheses for forced variability on submillennium time scales are effects of explosive volcanism and changes in solar energy output. Great uncertainty remains about their magnitude. Explosive volcanic eruptions generate large aerosol clouds in the stratosphere, where they perturb both incoming and outgoing radiation (10, 11). Generally, the former is the dominating effect and surface cooling occurs (12, 13). The bulk of the direct forcing for individual events is limited to a few years by the relatively short residence time of the injected particles in the lower stratosphere (14). Prolonged effects have been documented for temporally relatively closely spaced eruptions (15, 16), with feedbacks from reduced ocean heat content delaying the climatic recovery. However, damping mechanisms on the forcing might also exist for very large events (17).

There is an ongoing debate on the role of the sun in recent observed warming. Century-scale solar irradiance variations have been proposed as cause for past climatic changes (e.g., refs. 18 and 19). The latest summaries of the various uncertainties can be found in two recent reviews (20, 21). Satellite data since 1979 quantify the irradiance variations associated with the 11-year Schwabe sunspot cycle to ≈0.08–0.1% of the ≈1,367 $Wm^{-2}$ solar radiation reaching the top of our atmosphere (21). This variation translates into a radiative forcing of ≈0.2–0.3 W $m^{-2}$, roughly a factor of 10 smaller than the radiative forcing by well mixed greenhouse gases (2.4 W $m^{-2}$ in 2000 AD relative to 1750 AD). Although direct measurements of solar irradiance are limited to the satellite period (21), tentative correlations with records of sunspots (22, 23), aurora histories, geomagnetic indices, or the production rates of cosmogenic nuclei such as 10-Beryllium ($^{10}$Be) and radiocarbon ($^{14}$C) (3, 24) in conjunction with magnetic behavior of solar-like stars (25, 26) have been used to estimate solar irradiance in the past. The phase relationship between the isotopic records indicative of the sun's open magnetic field,

Author contributions: C.M.A., F.J., D.S.S., and B.L.O.-B. designed research; C.M.A. and F.J. performed research; C.M.A. contributed new reagents/analytical tools; C.M.A., F.J., D.S., and R.A.T. analyzed data; and C.M.A., F.J., D.S.S., and B.L.O.-B. wrote the paper.

The authors declare no conflict of interest.

Freely available online through the PNAS open access option.

Abbreviations: NH, Northern Hemisphere; NCAR CSM, National Center for Atmospheric Research Climate System Model.

‡To whom correspondence should be addressed. E-mail: joos@climate.unibe.ch.

This article contains supporting information online at www.pnas.org/cgi/content/full/0605064103/DC1.

sunspot numbers, and the sun's closed magnetic field or its total energy output is not fully understood (27). Nevertheless, the temporal evolution of the different proxy series, particularly in certain well defined frequencies (≈11-year Schwabe Cycle, ≈80- to 85-year Gleissberg Cycle, and ≈207-year deVries Cycle), is in reasonable agreement across most solar proxies (20, 28), and comparisons between proxies suggest significant modulation consistent with deduced solar cycles (20). However, the scaling required to translate a proxy record of sunspot number, or production rate of $^{10}$Be, into actual solar irradiance anomalies is highly uncertain, and published estimates of multidecadal solar irradiance changes vary by more than a factor of five (3, 21). Recently, astronomical evidence has been used to suggest that low-frequency variability of solar irradiance might be very low, possibly restricted to the range of the observed high-frequency variability (29, 30). These new estimates are lower by a factor of five or more than the upper end of previously used values (25, 31). Such low forcing from solar irradiance changes has even led to suggestions that low frequency paleoclimatic variability was not forced by solar variability.

We used a climate model to analyze paleoclimatic responses to solar and volcanic forcing, using a range of estimates of the magnitude of the solar forcing to bracket climate sensitivity to this variable. Possible transient effects of solar irradiance changes on climate have been investigated with computationally efficient models, such as Energy Balance Models (15, 32) and Models of Intermediate Complexity (33, 34) as well as with Atmosphere-Ocean-General Circulation Models for the 20th century (35) and the past (36, 37). Here, we employ a coupled Atmosphere–Ocean General Circulation Model in experiments covering the period of the last 1,150 years. The low-frequency solar forcing was taken from the Antarctic $^{10}$Be record of (3), following a widely accepted, but uncertain, approach also used in the most recent review of Foukal and collaborators (38). The $^{10}$Be record was scaled to solar irradiance over much of the published range. We identify links between the solar forcing and modeled temperature as well as proxy-based temperature reconstructions.

## Model and Forcings

Simulations for this study are conducted with the National Center for Atmospheric Research Climate System Model (NCAR CSM), Version 1.4, a global coupled atmosphere-ocean-sea ice-land surface model without flux adjustments (39, 40) [for a detailed description, see supporting information (SI) *Text*].

The model was forced over the period from 850 to 2000 AD using observation-based time histories of solar irradiance, spatially explicit aerosol loading from explosive volcanism, the greenhouse gases ($CO_2$, $CH_4$, $N_2O$, CFC-11, and CFC-12), and anthropogenic sulfate aerosols (Fig. 1) with a recurring annual cycle of ozone and natural sulfate aerosol. This setup is directly comparable to the host of climate change experiments that focus on the 20th century. Other forcing factors, such as orbital parameter changes (very slow forcing, we used constant 1400 AD conditions) and vegetation/land use changes (highly regional in its impact), were not included.

The solar irradiance history over the past 1,150 years was based on a recent $^{10}$Be history (3) recovered from Antarctica. Although the annual $^{10}$Be deposition might be affected by atmospheric circulation changes, the dominant multidecadal to centennial (Maunder Minimum-type) solar modulation estimates correspond closely to independent estimates based on $^{14}$C (20) and to a recent solar irradiance reconstruction with a flux transport model of the Sun's total magnetic flux (41), and therefore are thought to represent solar variability. The different estimates of past solar irradiance changes applied in the NCAR CSM used three very different estimates of the scale factor (Fig. 1). For two full-length (1,150-year) simulations solar irradiance was scaled to a reduction during the Maunder Minimum (1645–1715 AD) of 0.25% (23) and 0.65% (31) relative to present, representing a "medium" and a "high" case. Additionally, we performed a 450-year simulation from 1550 to 2000 AD applying a Maunder Minimum reduction scaling of 0.1% (29). This, for reasons of computational resource availability, shorter, "low" solar forcing simulation addresses recently raised doubts on the existence of any additional low-frequency trend in solar irradiance beyond the instrumentally measured variations of the 11-year cycle (26, 30).

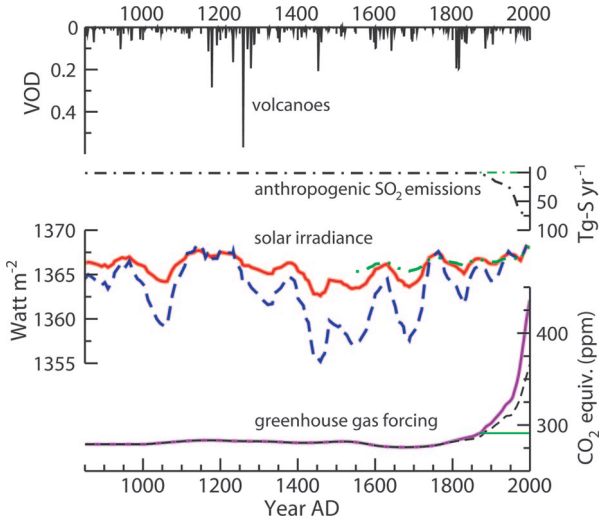


**Fig. 1.** Prescribed forcings. (*Top*) Volcanic forcing is indicated as global visible optical depth. (*Middle*) Solar forcing is obtained by scaling $^{10}$Be data of ref. 3 to a Maunder Minimum reduction in solar irradiance relative to today of 0.1% (green dash-dot, low solar simulation from 1550 to 2000 AD), 0.25% (red, solid, medium solar simulation from 850 to 2000 AD), and 0.65% (blue, dash, high solar simulation from 850 to 2000 AD). The 11-year solar cycle is not included in the forcing. Anthropogenic $SO_2$ emissions (dash-dot) and forcing by greenhouse gases (*Bottom*, solid), expressed as $CO_2$ equivalent, are from ref. 42. The atmospheric $CO_2$ concentration is shown by the black, dashed line. Three long simulations were run with prescribed solar (high, medium, and low scaling) and identical volcanic, greenhouse gas, and tropospheric sulfate forcing. In addition, three "natural-only" simulations were branched off from each long integration at year 1870 AD, with greenhouse gas concentrations and anthropogenic sulfate kept constant at 1870 AD levels (green lines).

The volcanic forcing was established by converting ice core aerosol proxies to latitudinal and temporally varying atmospheric aerosol fields following earlier work (16). Volcanic aerosol was specified as a single aerosol size distribution, and optical depth was scaled linearly with the aerosol loading. Atmospheric $CO_2$, $CH_4$, and $N_2O$ concentrations were individually prescribed following ice core measurements and direct atmospheric observations. The CFC-11, scaled to take into account the radiative forcing by other halogenated species and $SF_6$ (42), and CFC-12 concentration histories are based on historic emission data and recent measurements. The volcanic and anthropogenic forcing histories were the same in all three simulations.

The model was spun-up over two centuries using preindustrial forcings (see *SI Text* for a detailed description of the spin-up procedures), and a control experiment without any forcing changes (fixed at 850 AD conditions) was run in parallel to the forced experiments over the full period of 1150 years. This control exhibits a cooling in global-average surface temperature of 0.07°C per century over the first 600 years primarily resulting from the long adjustment time scale of the ocean; after 1500 AD, global average surface temperature have reached a quasi-

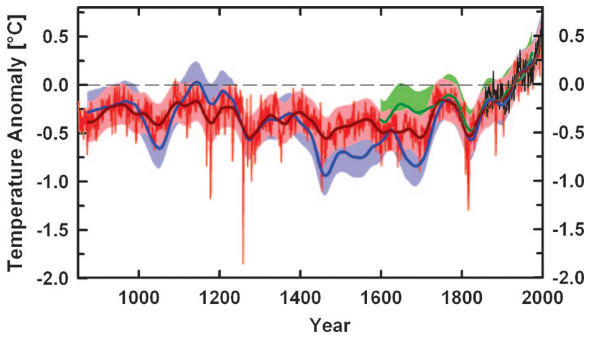


**Fig. 2.** Global average surface temperature (50-year Gaussian weighted average) simulated with the NCAR CSM 1.4 with prescribed high (blue), medium (red) and low (green) solar forcing. Annual data are shown for the medium solar forcing run (red, thin line) and for the instrumental record of global average surface temperature (ref. 50, black). Volcanic, greenhouse gas, and tropospheric sulfate forcing are the same in all three simulations. Shaded ranges depict two positive and negative standard deviations around the 50-year averages computed from 1,000 years of an unforced control simulation (SD = 0.107°C).

equilibrium. All results shown here are detrended residuals after subtracting a millennial-scale spline fit for individual months of the annual cycle at each model grid point obtained from the control integration. This process preserves all temporal structure below 1,000 years, but it might affect the overall millennial-scale signal separation.

The main experiments include the anthropogenic change in radiative forcing over the industrial period. To evaluate the contribution of natural forcing (solar and volcanic) to the 20th century climate change, additional simulations were performed over the period 1870 to 1999 AD with all anthropogenic forcings fixed at the 1870 AD values (Fig. 1). These simulations were directly branched-off the three main experiments to take into account the inertia of the climate system, and the influence of preindustrial forcing changes, on 20th century climate evolution.

## Results

Both simulations covering the full 1,150-years (Fig. 2) show a clear two-stage initial warming interrupted by a temperature drop in the 11th century. Relative maxima in global temperatures occur during the 10th century, as well as between the late 11th and the 12th century. Subsequently, modeled temperatures generally decrease. Globally, the coldest episodes are in the 15th and 17th centuries (high solar forcing), 13th, 15th, 17th, and 19th centuries (medium solar forcing), and the 19th century (low solar forcing, but based on a shorter run). Over the instrumental record after 1850 AD, all three runs are essentially indistinguishable and they closely match the observed large scale warming both in magnitude and in temporal evolution. In all three simulations, decadal-mean global average surface temperature was higher during the most recent three to four decades than during the previous 1,100 years. During the preindustrial period, the three experiments are generally separated by several tenths of a degree Celsius (Fig. 2). The difference is due to the changes in solar forcing magnitude because all other forcings were identical across the experiments. This difference is greater than one standard deviation of the low-frequency variability of the control run (0.11°C). Decadal-scale NH surface temperature is generally synchronous with the global-mean, but NH-perturbation amplitudes are larger by ≈20%.

Several sharp cooling episodes mark the response to very large volcanic forcing (e.g., 1258 AD, 1453 AD, 1815 AD). The largest volcanic forcing was estimated for 1258 AD (Fig. 1) after the probably largest explosive eruption of the past few thousand years. The source volcano of this event is still unknown, although bipolar sulfate deposition together with its consistent chemical signature (43) at around ≈1258 AD makes it clear that it is a tropical event. This particularly large event was followed by a remarkable sequence of large eruptions, causing a clear temperature decrease of several tenths of a degree Celsius over the late 13th century (Fig. 2). Similar cumulative volcanic cooling is also simulated in the mid-15th, 17th, the early 19th, and (to a lesser degree) the late 19th to early 20th century. Some of these volcanically active periods occur contemporaneous to solar induced cooling (e.g., Maunder Minimum) and thus make a clear separation of climate response at the low frequencies difficult.

The preindustrial range in multidecadal global surface temperature is reduced by more than a factor of two in the low and medium experiments compared with the high solar forcing case (Fig. 2). The amplitude difference between the warmest and coldest periods at the decadal time scale is ≈0.4°C (pre-1850) for the low and medium simulations as compared with ≈1°C for the high scaling. High scaling of the solar forcing yields both the coldest and warmest decades in all simulations before the 20th century. Even so, this largest scaling factor never generates a global, or hemispheric, temperature as large as those in the late 20th century.

There is a link between simulated low-frequency climate variability and the natural climate forcings during the preindustrial period. The correlation between solar forcing and modeled global surface temperature series decreases with diminishing solar forcing magnitude. Fifty-year long, Gaussian-weighted global surface temperature variations in the high-forcing experiment are almost entirely determined by the solar forcing (decadal data $r^2 = 0.88$, SI Fig. 5). This cause–effect link is reflected in a tight phase relationship in the dominant century-scale frequency band of solar variability (≈1/200 year, SI Fig. 6). The relationship between solar forcing and global surface temperature is reduced in the medium-forcing run ($r^2 = 0.47$). The solar forcing response becomes smaller relative to the model's internal variability, and the ratio of solar signal to volcanic influence and/or model noise decreases. Deviations of simulated temperature evolution from the evolution of irradiance do occur repeatedly, and are almost exclusively negative due to explosive volcanism (SI Fig. 5). The surface temperature response to individual volcanic eruptions is consistent with previous results (16), although several appear to be too large compared with many proxy-based estimates. This overestimate is not a result of the forcing series (the volcanic forcing in ref. 15 is very similar), but rather arises from the fixed aerosol size distribution used to represent volcanic sulfate. This method could produce particles that are probably too small, and thus radiatively too efficient, for cases where the loading of sulfate is very large.

The simulated decadal-scale NH temperature variations of the medium-scaled run fall mostly within the uncertainty band from the proxy-based reconstructions (Fig. 3*b*). Only during the cool interval within the Medieval Warm Period (≈1050 AD) do simulated temperatures fall below this range. Generally, the reconstructed high temperatures in the 11th and 12th centuries, and the cold conditions between 1450 and 1800 AD, are reflected in the model results. Relative minima and maxima found in the proxy reconstructions, such as those in the late 18th century and the beginning of the 19th century, or ≈1570 and 1450 AD, are also found in the medium-scaled simulation. For a comparison between modeled NH temperatures with various proxy reconstructions, see SI Fig. 7.

The results of the low and high solar forcing experiments encompass the (pre-1850) amplitude range in multidecadal-averaged NH temperatures of the available proxy reconstructions (Fig. 3*b*). The preindustrial amplitude of >1.1°C for NH-temperature found in the high solar forcing simulation is larger than in all reconstructions; however, the variations of up

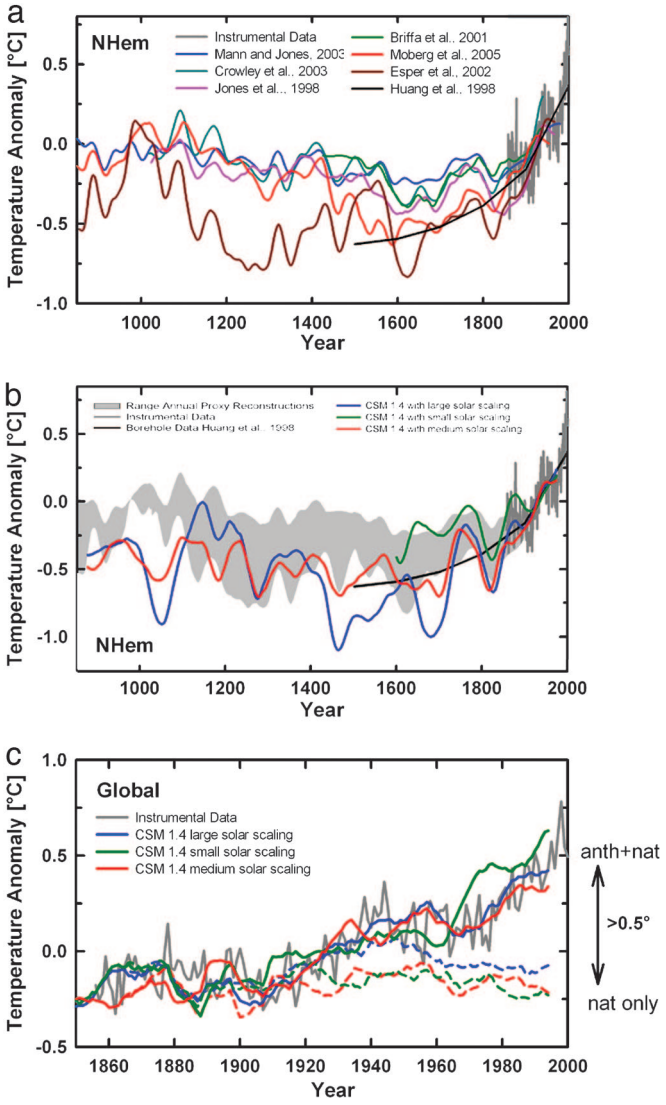


**Fig. 3.** Comparison of NCAR CSM simulations with proxy reconstructions and instrumental data. (*a*) Reconstructed NH average surface temperature anomalies over the past millennium (5–9, 51, 52). All series are as published originally and no additional scaling has been performed, but annual records have been smoothed with a 50-year-long Gaussian filter. All series are relative to 1901–1960 averages computed from original data. The instrumental series is from ref. 50 (dark gray). (*b*) Northern hemisphere surface temperature from the low- (green), medium- (red), and high-scaled (blue) solar forcing simulations compared with the range spanned by the annual proxy-based reconstructions (refs. 5, 7–9, 52, and 53; gray shaded area). This range does not include a systematic error analysis, it only illustrates the current debate regarding the amplitude of hemispheric multidecadal to century-scale temperature variations of the past. The smooth borehole-based estimate from ref. 54 is shown by the solid black line. Instrumental series, reference period, and filter as in *a*. (*c*) Simulated versus the instrumental (gray) record of global average surface temperature (gray, thick solid line). The time series of the low (green), medium (red), and high (blue) solar forcing experiments were smoothed by using an 11-year Gaussian filter. Anthropogenic forcings were included in the primary experiments (solid lines) but held at 1870 AD conditions in 1870–2000 AD branch experiments (dashed lines).

to 1°C proposed in refs. 6–8 are comparable to the modeled amplitude (values determined by using 50-year Gaussian running averages). However, the simulated cool periods (late 15th and 17th century, as well as the 11th century cooling) are significantly colder in the high-scaled CSM run compared with any of these reconstructions (Fig. 3*b*). The pre-1850 NH-

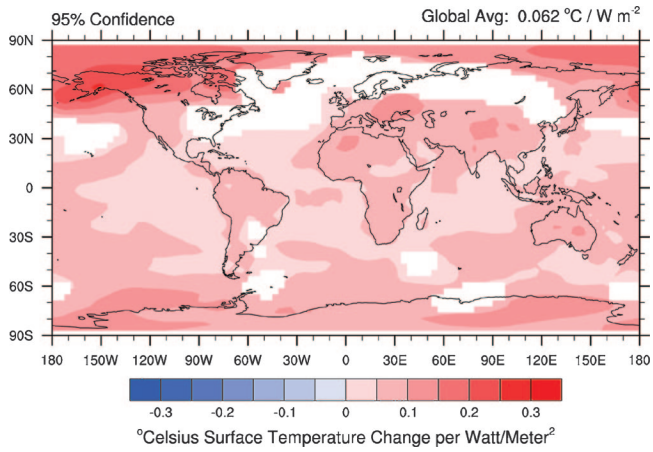


**Fig. 4.** The spatial pattern of solar-induced temperature changes in °C per W $m^{-2}$ for the medium solar forcing simulation over the period from 850 to 1849 AD. Values shown are determined by using linear regression of local annual temperature onto solar irradiance anomalies and are restricted to areas that pass significance tests with 95% confidence taking into account serial correlation of the time series. Global mean response (from significant areas only) is equivalent to 0.062°C for each W $m^{-2}$ irradiance change at the top of the atmosphere. High and low scaled solar forcing results are shown in SI Fig. 8.

temperature range of 0.4°C found in the low case is essentially the same as proposed in refs. 4 and 5.

Solar forcing and low-frequency volcanic forcing are anticorrelated around 1600 AD (Fig. 1). The $^{10}$Be and radiocarbon records (3, 20) suggest that solar forcing increases in the late 16th century to peak early in the 17th century, whereas volcanic eruptions tend to cool the Earth surface at the same time. All temporally resolved reconstructions exhibit NH cooling after ≈1570 AD (Fig. 3*a*). This is also the case in the medium-scaled run (Figs. 2 and 3). In contrast, simulated NH temperature in the high-scaled run continues to increase after 1570 AD until the peak in the $^{10}$Be solar forcing around 1620 AD. This finding suggests that the (high-scaled) prescribed solar forcing is too strong at that time, whereas there is no indication that the volcanic forcing would be underestimated. This direct effect of a very strong solar influence on the phase of the low-frequency variation is also illustrated in SI Fig. 6.

Turning to the instrumental record, all three simulations with anthropogenic forcing yield a 20th-century warming of ≈0.6°C (medium and high solar) to 0.7°C (low solar) (Fig. 3*c*). This finding is fully consistent with the data-based estimate of 0.6 ± 0.2°C, and the evolution of global-mean surface temperature very closely matches the instrumental record. The natural-only extensions for all three simulations after 1870 AD (holding greenhouse gases and tropospheric aerosol constant at 1870 AD conditions) yield a 20th century peak warming (decadally smoothed data) of ≈0.2°C, which visibly reduced by the end of the century through increased volcanism. The separation of a human-induced warming from the natural background temperature evolution occurs early in the 20th century in the model. By the end of the century, the difference in simulated global temperature response between natural and natural plus anthropogenic forcings is >0.5°C.

Fig. 4 shows the spatial pattern of regression coefficients for the relationship between solar forcing and temperature response. The patterns, although not a validation of the model, do show expected features, suggesting that in broad terms the model correctly captures the spatial impact of solar-induced temperature changes. The most prominent feature is the tendency to have more sensitivity (larger regression coefficients) over land than over the oceans (37), as expected due to the higher

heat-absorbing capacity of the oceans. The model result also exhibits polar amplification, or higher sensitivity at high latitudes, with a greater effect in the NH because of the interaction of this effect with the land-ocean contrast. However, because of a lack of interactive ozone, the model cannot fully simulate features discussed in (44). The Southern Hemisphere, with its sparser landmasses, shows less amplification. There is some variability in sensitivity within the NH high latitude regions, likely because of persistent climate patterns associated with planetary wave structure. Finally, there are some regions with only insignificant temperature response (including small areas with slight negative relationships) to solar forcing, mainly in the NH high latitude oceans. These represent regions of complex interactions between climate, ocean currents (particularly their position) and ocean heat uptake. However, part of the signal is associated with a known (probably unrealistic) internal oscillation in this area of the coupled model. Overall, the magnitude of temperature response to solar irradiance changes is relatively small. Global average temperatures change by ≈0.066 ± 0.005°C for each Watt per square-meter change in solar irradiance (with 0.066°C for the medium and 0.071°C for the high-scaled experiments).

## Discussion and Conclusions

We forced a set of transient millennium-long simulations with the NCAR CSM 1.4 coupled atmosphere-ocean-land-sea ice general circulation model with South Pole $^{10}$Be-based estimates of solar irradiance (3). The simulations were compared with temperature reconstructions and the instrumental record to investigate links between solar forcing and surface temperature change. Although $^{10}$Be records, indicative of the open magnetic field flux, are not without problems as direct representations for past solar irradiance (38), their temporal structure at the century time scale is closely matched by variations seen in other, independent proxies of solar activity (20) and a recent irradiance reconstruction (41). Thus, the dominant variations in the record represent actual changes related to the sun, and do not merely reflect potential climatic perturbations of the deposition process. However, the largest uncertainty in the low-frequency component of solar forcing mostly arises from its unknown amplitude. Using three different estimates of background changes in solar activity that encompass the published range allowed us to test if a large forcing amplitude is required to generate a detectable climate response, or if small amplitudes could also generate a discernable impact. Furthermore, the low (≈2°C) sensitivity of our climate model then offers the opportunity to further constrain the magnitude of the solar forcing amplitude. We found that small scaling-factors, resulting from low assumed amplitude of the solar forcing, generate meaningful global and hemispheric climate fluctuations.

Our results show that the different solar forcing amplitudes lead to a clear separation of the large-scale climate histories. Based on the solar origin of dominant $^{10}$Be fluctuations, the phase response in the NCAR CSM 1.4 on the global and hemispheric scale compared with large-scale climate reconstructions suggests that even low amplitude solar variations can affect climate on multidecadal to centennial time scales. The larger the amplitude of solar forcing, the more the effects of other natural forcings are suppressed (such as explosive volcanism or variations in atmospheric composition before ≈1800 AD). However, the rapidly increasing anthropogenic forcings dominate the simulations over the 20th century. Independent of the magnitude of solar forcing, and thus independent of the magnitude of prior cooling, no significant difference is seen in the simulations over this period. Our model results also suggest that the climate response to slow variations in forcing occur with relatively little time lag (see SI Fig. 5).

We use the ensemble of available proxy-reconstructions to define a range of past, decadal-scale NH temperature variability to gauge our model results. While the NH temperatures of the high-scaled experiment are often colder than the lower bound from proxy data, the modeled decadal-scale NH surface temperature for the medium-scaled case falls within the uncertainty range of the available temperature reconstructions. The medium-scaled simulation also broadly reproduces the main features seen in the proxy records. The timing (phasing), and to some degree the magnitude, of local minima and maxima found in the proxy NH temperature reconstructions are also evident in the simulation, showing that in the context of a climate model, a discernable solar signal is possible with medium solar forcing amplitudes. The (shorter) low-scaled simulation produced NH temperature variations in good agreement with the low end of the proxy range, but a clear solar signal is difficult to identify (global numbers are not significant), because volcanic forcing is now primarily responsible for natural climate variations. A high-latitude spatial (planetary wave) response to solar forcing similar to earlier Atmosphere–Ocean General Circulation Model studies (37, 44) has been identified, although caveats arising from an internal oscillation in the coupled system need to be kept in mind.

The ensemble obtained by running the NCAR CSM with three different natural forcing histories encompasses the published range of naturally forced low frequency NH-temperature variations over the past 1,150 years. This conclusion holds irrespective whether in reality the temperature variations were caused by irradiance changes and volcanic eruptions alone or in combination with indirect solar mechanisms, such as solar-induced changes in stratospheric ozone and associated circulation changes (44, 45) or through modification of cloud properties (46, 47). Given the recent arguments suggesting low amplitude solar variation, it is interesting that the high solar forcing appears to be incompatible with observations. Both the phase relationships and magnitude between reconstructed and simulated temperatures in the dominant solar frequency band of ≈1/200 years break down with high solar forcing. Given the low climate sensitivity of the NCAR CSM, a large (0.65%) background change in solar irradiance over past centuries appears unlikely. The comparison of the model results with the proxy based reconstructions suggest that smaller, and possibly much smaller irradiance changes are more consistent with most of the available temperature reconstructions both in magnitude and phase, particularly if the real world climate sensitivity is significantly higher than the NCAR CSM's. The climate model results exhibit a response of 0.066 ± 0.005°C in global temperature for each Watt per square-meter change in solar input. This result implies that for small irradiance changes (29, 38) (<2 $Wm^{-2}$) solar induced temperature variation would probably be limited to 0.1–0.15°C, or <0.2°C if a higher climate sensitivity were considered. Although a solar contribution can be isolated in the model results, its relative role diminishes with reduced amplitudes and the contribution of solar forcing to natural variability becomes small. A relatively small climate change (<1°C) of NH surface temperatures is also consistent with the small preindustrial variations in atmospheric $CO_2$, $CH_4$, and $N_2O$ and an independent estimate based on atmospheric greenhouse gas changes over the past millennium (32, 48). This result is particularly robust because of the low sensitivity of the model.

Without anthropogenic forcing, the 20th century warming is small. The simulations with only natural forcing components included yield an early 20th century peak warming of ≈0.2°C (≈1950 AD), which is reduced to about half by the end of the century because of increased volcanism. This trajectory is similar for all magnitudes of solar irradiance change or the magnitude of cooling before. High scaling of the solar irradiance leads to model temperatures by the end of the century that are only

marginally (≈0.1°C) warmer than those from the low and medium scaled forcing. This finding suggests that, while solar irradiance changes and explosive volcanism were the dominant forcings in preindustrial times, their combined role has been changing over the past century. Although these natural forcing factors could be responsible for some modification of the decadal structure over the 20th century, they only played a minor role in the most recent warming. Therefore, the 20th century warming is not a reflection of a rebound from the last Little Ice Age cool period, but it is largely caused by anthropogenic forcing. A small role of solar forcing for late 20th century climate change is additionally supported by the absence of a trend in the satellite-based irradiance record covering the past 30 years (21). By the end of the 20th century, global temperatures simulated with natural and anthropogenic forcings included are >0.5°C warmer than if only natural factors are allowed to change after 1870 AD. A larger climate sensitivity would simply change the amplitudes but not the relative shape of the results, and thus yield a much larger than reconstructed preindustrial temperature variability for the experiment with high-scaled solar forcing. Inclusion of other forcing factors, such as absorbing aerosols as well as the indirect aerosol effect, would probably change little in the relative difference between the natural and the combined natural plus anthropogenic forcing experiments. Probabilistic approaches considering uncertainties in aerosol and other forcings indicate that 20th century anthropogenic forcing is much larger than solar forcing (49).

In conclusion, our model results indicate that the range of NH-temperature reconstructions and natural forcing histories (cosmogenic isotope record as a proxy for solar forcing, and volcanic forcing) constrain the natural contribution to 20th century warming to be <0.2°C. Anthropogenic forcing must account for the difference between a small natural temperature signal and the observed warming in the late 20th century.

We are grateful for comments and suggestions by three anonymous reviewers that helped to clarify and sharpen the focus of the manuscript. We thank E. Dlugokencky, J. Flückiger and A. Dällenbach for providing greenhouse gas data from the National Oceanographic and Aeronautic Administration (NOAA)/Climate Monitoring and Diagnostics Laboratory air-sampling network and from ice cores, as well as the International Geosphere–Biosphere PAGES/World Data Center for Paleoclimatology and NOAA/National Climactic Data Center Paleoclimatology Program (Boulder, CO) for providing climate reconstruction data. The National Center for Atmospheric Research is sponsored by the National Science Foundation. F.J. acknowledges support by the University of Bern, the Swiss National Science Foundation, and the University Corporation of Atmospheric Research/National Center for Atmospheric Research (NCAR) visitor program. Computing was done at NCAR with support from a special allocation from the NCAR Directors Reserve.

1. Jones PD, Mann ME (2004) *Rev Geophys* 42:RG2002.
2. Robock A, Free MP (1996) in *NATO ASI Series*, eds Jones PD, Bradley RS, Jouzel J (Springer, Berlin), Vol I41, pp 533–546.
3. Bard E, Raisbeck G, Yiou F, Jouzel J (2000) *Tellus B* 52:985–992.
4. Mann ME, Bradley RS, Hughes MK (1998) *Nature* 392:779–787.
5. Mann ME, Jones PD (2003) *Geophys Res Lett* 30:1820.
6. Huang SP, Pollack HN, Shen PY (2000) *Nature* 403:756–758.
7. Esper J, Cook ER, Schweingruber FH (2002) *Science* 295:2250–2253.
8. Moberg A, Sonechkin DM, Holmgren K, Datsenko NM, Karlen W (2005) *Nature* 433:613–617.
9. Jones PD, Briffa KR, Barnett TP, Tett SFB (1998) *Holocene* 8:455–471.
10. Stenchikov GL, Kirchner I, Robock A, Graf HF, Antuna JC, Grainger RG, Lambert A, Thomason L (1998) *J Geophys Res* 103:13837–13857.
11. Lacis AE, Hansen JE, Sato M (1992) *Geophys Res Lett* 19:1607–1610.
12. Robock A (2000) *Rev Geophys* 38:191–219.
13. Briffa KR, Jones PD, Schweingruber FH, Osborn TJ (1998) *Nature* 393:450–455.
14. Robock A, Mao J (1993) *J Climate* 8:1086–1103.
15. Crowley TJ (2000) *Science* 289:270–277.
16. Ammann CM, Meehl GA, Washington WM, Zender CS (2003) *Geophys Res Lett* 30:1657.
17. Pinto JP, Turco RP, Toon OB (1998) *J Geophys Res* 94:165–174.
18. Eddy JA (1976) *Science* 192:1189–1202.
19. Fleitmann D, Burns SJ, Mudelsee M (2003) *Science* 300:1737–1739.
20. Muscheler R, Joos F, Beer J, Müller SA, Vonmoos M, Snowball I (2007) *Q Sci Rev* 26:82–97.
21. Fröhlich C, Lean J (2004) *Astron Astrophys Rev* 12:273–320.
22. Hoyt DV, Schatten KH (1993) *J Geophys Res* 98:18895–18906.
23. Lean J, Beer J, Bradley R (1995) *Geophys Res Lett* 22:3195–3198.
24. Stuiver M, Braziunas TF (1989) *Nature* 338:405–408.
25. Baliunas S, Jastrow R (1990) *Nature* 348:520–522.
26. Hall JC, Lockwood GM (2004) *Astrophys J* 614:942–946.
27. Wang Y-M, Sheeley NR (2003) *Astrophys J* 591:1248.
28. Muscheler R, Joos F, Müller SA, Snowball I (2005) *Nature* 436:E3–E4.
29. Lean JL, Wang YM, Sheeley NR (2002) *Geophys Res Lett* 29:2224.
30. Foukal P, North G, Wigley T (2004) *Science* 306:68–69.
31. Reid GC (1997) *Climatic Change* 37:391–405.
32. Gerber S, Joos F, Brugger P, Stocker TF, Mann ME, Sitch S, Scholze M (2003) *Climate Dyn* 20:281–299.
33. Bertrand C, Loutre MF, Crucifix M, Berger A (2002) *Tellus Ser A* 54:221–244.
34. Bauer E, Claussen M, Brovkin V, Huenerbein A (2003) *Geophys Res Lett* 30:1276.
35. Meehl GA, Washington WM, Wigley TML, Arblaster JM, Dai A (2003) *J Climate* 16:426–444.
36. Gonzalez-Rouco F, von Storch H, Zorita E (2003) *Geophys Res Lett* 30:2116.
37. Cubasch UR, Voss R, Hegerl GC, Waszkewitz J, Crowley TJ (1997) *Climate Dynamics* 13:757–767.
38. Foukal P, Fröhlich C, Spruit H, Wigley TML (2006) *Nature* 443:161–166.
39. Otto-Bliesner BL, Brady EC (2001) *J Climate* 14:3587–3607.
40. Boville BA, Kiehl JT, Rasch PJ, Bryan FO (2001) *J Climate* 14:164–179.
41. Wang YM, Lean JL, Sheeley NR (2005) *Astrophys J* 625:522–538.
42. Joos F, Prentice IC, Sitch S, Meyer R, Hooss G, Plattner G-K, Gerber S, Hasselmann K (2001) *Global Biogeochem Cycles* 15:891–907.
43. Palais JM, Germani MS, Zielinski GA (1992) *Geophys Res Lett* 19:801–804.
44. Shindell DT, Schmidt GA, Mann ME, Rind D, Waple A (2001) *Science* 294:2149–2152.
45. Haigh JD (1994) *Nature* 370:544–546.
46. Svensmark H, Friis-Christensen E (1997) *J Atmos Sol Terr Phys* 59:1225–1232.
47. Tinsley BA (2000) *Space Sci Rev* 94:231–258.
48. MacFarling Meure CM (2004) PhD thesis (Melbourne Univ, Melbourne, Australia).
49. Knutti R, Stocker TF, Joos F, Plattner GK (2002) *Nature* 416:719–723.
50. Jones PD, Moberg A (2003) *J Climate* 16:206–223.
51. Crowley TJ, Lowery TS (2000) *Ambio* 29:51–54.
52. Briffa KR, Osborn TJ, Schweingruber FH, Harris IC, Jones PD, Shiyatov SG, Vaganov EA (2001) *J Geophys Res* 106:2929–2941.
53. Crowley TJ, Baum SK, Kim KY, Hegerl GC, Hyde WT (2003) *Geophys Res Lett* 30:1932.
54. Huang SP, Pollack HN (1998) in *Contrib Ser 1998–044, IGBP Pages/World Data Cent A for Paleoclimatol Data* (NOAA/NGDC Paleoclimatol Program, Boulder, CO).